Predictability of South China Sea summer monsoon onset

Article

Accepted Version

Predictability of South China Sea Summer Monsoon onset

Gill M. MARTIN[1*], Amulya CHEVUTURI[2], Ruth E. COMER[1], Nick J. DUNSTONE[1], Adam A. SCAIFE[1,3], and Daquan ZHANG[4]

[1]*Met Office Hadley Centre, Met Office, FitzRoy Road, Exeter, EX1 3PB, UK*

[2]*NCAS-Climate and Dept. of Meteorology, University of Reading, Reading, RG6 6BB, UK*

[3]*College of Engineering, Mathematics and Physical Sciences, Exeter University, Exeter, EX4 4QJ, UK*

[4]*Laboratory for Climate Studies, National Climate Center, China Meteorological Administration, Beijing 100081, China*

ABSTRACT

Predicting monsoon onset is crucial for agriculture and socioeconomic planning in countries where millions rely on the timely arrival of monsoon rains for their livelihoods. In this study we demonstrate useful skill in predicting year to year variations in South China Sea summer monsoon onset at up to 3 months lead time using the GloSea5 seasonal forecasting system. The main source of predictability comes from skilful prediction of Pacific sea surface temperatures associated with El Niño and La Niña. The South China Sea summer monsoon onset is a known indicator of the broadscale seasonal transition that represents the first stage of the onset of the Asian summer monsoon as a whole. Subsequent development of rainfall across East Asia is influenced by sub-seasonal variability and synoptic events that reduce predictability, but interannual variability in the broadscale

*Corresponding author : Gill MARTIN
Email: gill.martin@metoffice.gov.uk

monsoon onset for East Asian summer monsoon still provides potentially useful information for users about possible delays or early occurrence of the onset of rainfall over East Asia.

Key words: SCSSM, South China Sea Summer Monsoon, EASM, East Asian Summer Monsoon

1. Introduction

The broadscale East Asian Summer Monsoon (EASM) onset occurs in two stages (Wang et al, 2004; 2009): The first stage is a seasonal transition that occurs over the South China Sea (SCS) and is characterised by an abrupt but sustained reversal of the lower tropospheric zonal winds from easterlies to westerlies. Several studies have considered the SCS Summer Monsoon (SCSSM) onset as the precursor for the EASM development (Tao and Chen, 1987; Lau and Yang, 1997), with the formation and progression of the mei-yu rainband forming the second salient phase (Wang et al., 2004). Predicting monsoon onset is crucial for agriculture and socioeconomic planning in countries where millions rely on the timely arrival of monsoon rains for their livelihoods.

Interannual variability in the seasonal transition that constitutes the broadscale monsoon onset has been shown to be related to thermal conditions over the Tibetan Plateau (Wu et al., 2012), El Niño-Southern Oscillation (ENSO) effects (Zhou and Chan, 2006; Hu et al., 2014; Xie et al., 2015; Zhu and Li, 2017), regional air-sea interactions (He and Wu, 2013) and intraseasonal oscillations (ISO; Li et al., 2013; Wu 2010; Zhu and He, 2013; Shao et al., 2014; Wang et al., 2017). He et al. (2017) carried out a comprehensive analysis

of the SCSSM onset in individual years between 1997 and 2014 and showed that the years can be divided into “normal”, “intermittent” and “delayed” onset years based on the development of local circulations, thermodynamic conditions and rainfall patterns following the seasonal transition. He et al. (2017) found that eight out of the 18 years they analyzed exhibited intermittent rainfall onset (such that the seasonal dynamical transition is not closely followed by the establishment of monsoon rains and maximum SCS surface temperatures, with a delay caused by an active ISO or northern cold air entering the SCS), and suggested that this reduces the potential predictability of local rainfall onset even if the seasonal dynamical transition may be predictable. Wang et al. (2017) described the effects of the tropical ISO on early, normal and late SCSSM onsets observed over 34 years. They confirmed work from previous studies which showed that, before each onset, the SCS is controlled by the dry phase of the ISO (Shao et al., 2014), and the SCS is warmed to precondition the onset, while after each onset, the SCS is cooled by the wet phase of the ISO (Wu, 2010). However, Wang et al. (2017) showed that the transition process is found to be related to different ISO evolutions over the Indian Ocean for the three types of onsets.

Even in non-intermittent onset years, the progression of rainfall onset over East Asia is rarely smooth. After an initial burst of rainfall over the SCS, the rain band rapidly advances northward before stagnating over the Yangtze and Huai River valleys in the mei-yu front (baiu in Japan). The mei-yu rainband exhibits large intra-seasonal and interannual variability and has been the subject of extensive literature (see Ding and Chan (2005) for a review). Its onset is associated with a northward shift of the Northwest Pacific Subtropical High axis to about 25°N and the migration of the upper level westerly jet over Eurasia to the north of the Tibetan Plateau (Sampe and Xie, 2010; Luo 2013). Li et al. (2018) showed

that the anticyclone in the upper troposphere over South Asia in April has a significant relationship with the mei-yu onset dates, such that a stronger South Asian anticyclone in April is followed by earlier onset dates of the mei-yu.

Despite the complexity associated with these multiple drivers, interannual variability in the seasonal transition that constitutes the broadscale monsoon onset for the Asian summer monsoon as a whole still provides useful information for forecasters about possible delays or early occurrence of the onset of rainfall over East Asia. One of the most-used indices for determining SCSSM onset is that proposed by Wang et al. (2004). This index identifies the first pentad after 25th April in which the zonal wind at 850 hPa over the southern part of the South China Sea (5°-15°N,110°-120°E) shifts from a mean easterly to a mean westerly. Wang et al. (2004) demonstrate that this index is highly indicative of the seasonal transition of the large-scale circulation. They showed that the onset variations determined using this index matched the broadscale onset determined by the principal component of the first empirical orthogonal function (EOF) of the low level winds over East Asia and the Western North Pacific. They argued that this simple index avoids the additional complications of the intraseasonal variability that is included in EOF analysis.

An alternative definition for SCSSM onset was proposed by Gao et al. (2001), and is used in operational extended-range forecasting by the Chinese Meteorological Administration (D. Zhang, personal communication). This includes an additional criterion of a sustained increase of equivalent potential temperature at 850 hPa above 340K over the SCS region 10°-20°N, 110°-120°E concurrent with the establishment of westerly winds over the same region. The increase in equivalent potential temperature is considered to indicate sea surface warming, monsoonal transport of moisture into the region and the

potential for increased convective activity (Gao et al., 2001; Luo et al., 2013; Li et al., 2013). The region specified by Gao et al. (2001) is further north than that for the Wang et al. (2004) index and includes the northern SCS.

In this paper, we investigate the prediction skill of the SCSSM onset on seasonal timescales in the operational hindcast set of the GloSea5-GC2 seasonal forecasting system. Section 2 outlines the data and methods used in our study; section 3 shows the analysis of predictability of the two onset indicators, including tests of the robustness of the seasonal forecast skill. Discussion and conclusions on the usefulness of the seasonal forecast skill of the broadscale monsoon onset using these SCSSM onset indicators are included in Section 4.

2. Data and methods

Daily and pentad timeseries of 850 hPa zonal winds (U_{850}), air temperature (T_{850}) and specific humidity (q_{850}) from the 23-year set of hindcasts (1993-2015) made with the GloSea5-GC2 operational long-range forecast system (MacLachlan et al, 2015; Williams et al., 2015) are taken from four start dates (17th, 25th March, 1st, 9th April). This represents a >1-month lead-time for the average SCSSM onset date of mid-May. The standard operational hindcast set includes 7 members per start date. In order to investigate the robustness of our results, and the dependence on ensemble size, we make use of an additional hindcast ensemble, using the same model configuration and also with 7 members per start date (except for 17th March, for which there are only 3 members). Further, to investigate changes with lead-time, we repeat the analysis for a 56-member ensemble of start dates 25th March, 1st, 9th, 17th April, and for 28-member ensembles generated using the four start dates (1st, 9th, 17th, 25th) of January, February and March respectively.

Data representative of observations are taken from ERA-Interim reanalyses (Dee et al., 2011) for the same years. Equivalent potential temperature is calculated from the temperature and humidity fields at 850 hPa using the formula in Bolton (1980). Sea surface temperatures for March (used in section 3.3) are taken from the HadISST1.1 dataset (Rayner et al., 2005).

SCSSM onset is determined using the criteria established by Wang et al. (2004) and Gao et al. (2001). According to Wang et al. (2004), the onset date is the first pentad after 25th April (i.e. pentad 24 onwards) when the area-averaged U_{850} over the southern SCS (5°-15°N, 110°-120°E, denoted U_{SCS}) is (a) > 0 m s^{-1}; (b) in the subsequent four pentads (including the onset pentad) U_{SCS} must be positive in at least three pentads, and (c) the accumulated 4-pentad mean U_{SCS} > 1 m s^{-1}. Wang et al (2004), He and Zhu (2015) and Zhu and Li (2017) have compared the SCSSM onset pentads between different reanalyses (including the National Centers for Environment Prediction (NCEP) reanalyses versions I (Kalnay et al., 1996) and II (Kanamitsu et al., 2002) as well as ERA-Interim) and show reasonable correlations between them (generally >0.8).

Gao et al. (2001) suggested an onset criterion based on the area-averaged 850 hPa pentad equivalent potential temperature (θ_e) and U_{850} over the region 10°-20°N, 110°-120°E, with the onset date being the first pentad when θ_e > 340K[†] and the U_{850} > 0.0 m s^{-1} stably (persists for at least three pentads followed by a break of no more than 2 pentads, or for two pentads followed by a break of no more than one pentad). It should be noted that the region of consideration for this index is slightly further north than that considered by Wang et al. (2004).

[†] Originally specified as 335K by Gao et al. (2001) but revised to 340K by Ding and He (2006).

3. Results

3.1 Prediction skill of SCSSM onset using the Wang et al. (2004) criterion

Figure 1 shows the SCSSM onset pentads identified using the Wang et al. (2004) criterion for each forecast member with start dates 17th, 25th March, 1st, 9th April in each year, with the ensemble mean pentad and that identified in the reanalyses. The average interannual standard deviation of onset dates from individual ensemble members is 2.2 pentads, which compares reasonably well with that of the reanalyses (2.6 pentads), and there is a statistically significant (at the 0.75% level, for a one-tailed t-test) correlation of 0.5 between the interannual variations of the ensemble mean dates and those from the reanalyses, indicating significant predictability. The hindcasts also predict the mean onset pentad to match that of the reanalyses, i.e. pentad 28 (16th - 20th May).

Luo and Lin (2017) suggest that a more objective measure of the SCSSM onset can be determined using a daily cumulative U_{SCS} and specifying the onset as where this time series changes from decreasing to increasing (indicating that the flow is becoming predominantly westerly). Wang et al. (2004) also checked their SCSSM onset dates against a cumulative U_{SCS} criterion, DU, which compares the accumulated U_{SCS} in the 3 days prior to and after the onset. They showed that although their onset criteria do not explicitly require an abrupt change in westerly speed across the onset pentad, the resultant onset pentads were coincident with such a change. We find that including the additional criterion of DU > 7 m s^{-1} makes very little difference to our results (not shown).

We have carried out the same analysis for four start dates (1st, 9th, 17th, 25th) in January, February and March taken from the standard operational hindcast ensemble of 7 members per start date, and also for a 56 member combined ensemble using start dates of 25th March,

158 1st, 9th and 17th April (see Table 1). The correlation coefficient increases with decreasing
159 lead-time, becoming statistically significant at the 1.5% level (for a one-tailed t-test) from
160 February start dates onwards. Thus, there is significant skill in the SCSSM onset prediction
161 using the Wang et al. (2004) index at nearly 3 months lead-time over this hindcast period.

162 ***3.2 Predictability of SCSSM onset using the Gao et al. (2001) criterion***

163 Figure 2 shows the SCSSM dates identified using the Gao et al. (2001) criterion in
164 each year by each of the 52 ensemble members with start dates 17th, 25th March, 1st, 9th
165 April, with the ensemble mean pentad and that identified in the reanalyses. In contrast with
166 the findings using the Wang et al. (2004) U_{SCS} index, we find low skill in onset prediction
167 using the Gao et al. (2001) index at >1 month lead time. Table 1 shows that the correlation
168 increases slightly if the lead-time is reduced to ~1 month, but remains barely statistically
169 insignificant at the 6% level (using a one-tailed t-test).

170 The difference in prediction skill between the two methods of determining SCSSM
171 onset may be in part related to the region used for the Gao et al. (2001) index; Wang et al.
172 (2004) commented that *"the northern SCS is open to the invasion of a cold front from the*
173 *north. The westerly flow occurring before the onset is located north of the subtropical ridge*
174 *and is not of tropical origin."* They state, therefore, that the northern part of the SCS should
175 be excluded when defining the tropical monsoon burst over the SCS. He et al. (2017) also
176 commented on the influence of northern cold air entering this region of the SCS
177 contributing to ambiguous or intermittent onset. They highlighted the case of 2009, where
178 the strong westerly flow established in mid-April was interrupted by easterlies propagating
179 from the northern SCS for several days in early May. Other examples of years where this
180 occurred were given in He et al. (2017, their Figures 1, 2) and include 2007, 2009, 2011.

Additionally, although He et al (2017) did not identify 2004 as an intermittent onset year, the U_{850} averaged over the Gao et al. (2001) SCS box fluctuates between easterly and westerly during May, making the onset ambiguous when the Gao et al. (2001) index is used. He et al. (2017, their Figure 1) shows that this is related to variability of the winds in the northern part of the SCS. In contrast, the U_{850} winds over the southern part of the SCS (as covered by the Wang et al. (2004) box) do not fluctuate to the same extent. Chan et al. (2000) showed that, in 1998, incursion of cold air into the northern SCS promoted release of convectively available potential energy which helped to trigger the onset earlier than may have been expected given the ENSO conditions. Liu et al. (2002) further linked the cold air incursion to a Rossby wave train triggered over the Bay of Bengal.

The additional influence of variability from the subtropics in the northern SCS, which, like the ISO, is unpredictable on seasonal timescales, is likely to be a contributing factor in the reduced seasonal prediction skill for SCSSM onset using the Gao et al. (2001) criteria. In recognition of this, forecasters at CMA release their SCSSM onset forecasts using the Gao et al. (2001) criteria only on the extended range (11-30 day) timescale (D. Zhang, personal communication, 30th March 2018), on which models have been show in previous work to have skill for predicting intraseasonal variability (e.g. Lim et al., 2018; Lee et al. 2015).

3.3 Drivers of SCSSM onset predictability using Wang et al. (2004) index

Several studies have shown that ENSO is one of the main drivers of large-scale interannual variability in the Asian monsoon region (e.g. Zhou and Chan, 2007; Luo et al., 2016). Westerly (easterly) equatorial wind anomalies associated with El Niño (La Niña) and a weaker (stronger) Walker circulation are typically associated with negative (positive)

sea surface temperature (SST) anomalies over the SCS and a delayed (advanced) seasonal transition (He et al., 2017). This relationship is not symmetrical, however: He et al. (2017) suggest that both intraseasonal oscillations (ISO) and changes in west–east thermal contrasts across the Indian Ocean and western Pacific can influence the timing of onset in La Nina years. Hardiman et al. (2018) found a similar asymmetry in the relationship between seasonal mean Yangtze River rainfall and ENSO in observations and hindcasts.

We also show on Figure 1 the observed March Niño3.4 sea surface temperature (SST) anomaly timeseries from HadISST1.1 (yellow line). The correlation coefficient between the ensemble mean SCSSM onset pentad timeseries derived using the Wang et al. (2004) index and the Niño3.4 SST timeseries is 0.9, indicating that the predictable component of the hindcast SCSSM onset is driven mainly by ENSO, which itself is highly predictable on this timescale in GloSea5 (MacLachlan et al., 2015; Scaife et al., 2014). The correlation between observed estimates of SCSSM onset and the observed March Niño3.4 SST is rather lower (0.41), indicating the influence of other drivers of SCSSM onset variability that may not be predictable, particularly the ISO (e.g. Shao et al., 2014; Wang et al., 2017), which is itself subject to inter-annual variations relating to large-scale modes such as the Pacific-Japan teleconnection (Li et al., 2014). The skill of the ensemble (0.5) is therefore marginally higher than using predicted ENSO conditions alone to predict monsoon onset, though both are skilful.

Figure 3(a) provides additional insight by showing the correlation between the ensemble mean SCSSM onset dates for the 23 years from the hindcast and observed global monthly mean SSTs in March over the same period. This illustrates that the predictable part of the SCSSM onset from the hindcast is strongly correlated with an ENSO-like pattern

of Pacific SSTs, consistent with the findings of Zhu and Li (2017). There is also a strong positive correlation with SSTs in the equatorial Indian Ocean, again indicating that warmer SSTs are associated with later SCSSM onset dates. For the observed onset dates derived from ERA-interim (Fig. 3(b)), the correlations with SST are far smaller, due to the presence of additional factors in the observations that are not predicted by the ensemble mean. The average correlations between the SSTs and 1000 pseudo-timeseries of SCSSM onset created by randomly choosing an individual ensemble member hindcast for each year (Fig. 3(c)) are naturally smaller than with the ensemble mean timeseries, but not as low as those in observations (Fig. 3(b)). This suggests that some of the sub-seasonal variations (e.g. intraseasonal oscillations) that affect SCSSM onset in reality may not be sufficiently well represented by the model to capture such influences, even at the relatively high horizontal resolution used by GloSea5 (N216; about 60 km at 50°N). This is consistent with findings of Fang et al. (2016), who showed that while several aspects of the boreal summer ISO were improved in the Met Office Unified Model at this resolution, difficulty remained in realistic representation of the variance and propagation characteristics.

3.4 Robustness of SCSSM wind onset predictability to ensemble size

To assess the influence of ensemble size on the prediction skill using the Wang et al. (2004) index, we randomly sample small ensembles of between 1 and 51 members from the 52 members in our combined ensembles with start dates between 17th March and 9th April, and re-calculate the correlation between the ensemble-mean timeseries and that from the observations for different numbers of ensemble members. Figure 4 indicates that, for this measure of monsoon onset, the prediction skill (black line) rises quickly with ensemble size, reaching a mean value of 0.5 for a 28-member ensemble (which is the size of the

standard operational hindcast set), and is robust (correlation coefficients averaged over all ensemble-mean timeseries are statistically significant at the 1% level for a one-tailed test) for around 10 ensemble members or more. This is a reflection of the strong and predictable influence of ENSO on wider tropical rainfall (Kumar et al., 2013; Scaife et al, 2017) and here on the SCSSM onset dates in the hindcast: in most of the summers following strong El Niño/La Niña years (e.g. 1998, 1999, 2000, 2001, 2005, 2008, 2010) the spread among ensemble members is small and several members identify the same onset pentad (see Figure 1), thereby constraining the values selected by random sampling of the ensemble for those years.

Several authors (e.g. Scaife et al., 2014; Eade et al., 2014; Dunstone et al., 2016) have demonstrated that the model's North Atlantic Oscillation is less predictable than that observed, so that a large number of ensemble members is required for good prediction skill. This was confirmed by repeatedly randomly selecting a single member to be the truth and using the ensemble mean of the remaining members to predict that member. In contrast, the dashed line on Figure 4 indicates that the model's SCSSM onset dates are more predictable than those from reanalyses, *i.e.* that the model is *over-confident* in its predictions, as is often found for tropical rainfall (Weisheimer and Palmer, 2014). This again illustrates the dominant role of ENSO in providing the predictability in the model, while the observed onset dates are also influenced by intraseasonal variations that are unpredictable on the seasonal timescale.

4. Conclusions

SCSSM onset, as determined by the Wang et al. (2004) U_{850} wind index, is skilfully predicted in GloSea5 at up to 3 months lead time, particularly during active ENSO years.

Since the SCSSM onset signifies the start of the broadscale EASM, its skilful prediction is important for forecasters as an indicator of the possible characteristics of the season to come. This complements the skill previously demonstrated for predicting seasonal mean precipitation in the Yangtze River region (Li et al., 2016). The prediction skill for SCSSM onset using this index is robust even with only around 10 ensemble members, consistent with skill in prediction of rainfall in the deep tropics (e.g. Scaife et al., 2017). The skill is largely related to ENSO SSTs which have been shown to be highly predictable in the GloSea5 seasonal forecasting system.

In contrast, the Gao et al. (2001) SCSSM onset index, which includes an increase of θ_e in the SCS region as a measure of thermodynamic onset alongside the change to westerly winds, shows little predictability on seasonal timescales. We speculate that this is partly due to the region used by Gao et al. (2001), as this includes the northern SCS which can be influenced by incursions of cold air from the north. This additional influence is, like the ISO, inherently unpredictable on the seasonal timescale, and thus its inclusion through the northward extension of the box used for the Gao et al. (2001) index compared with that of Wang et al. (2004) is, in our view, a contributing factor in the reduced seasonal prediction skill. However, we propose that a seasonal forecast of the broadscale transition using the Wang et al. (2004) index would provide some useful early information for forecasters, and their guidance could later be refined, using other measures such as the Gao et al. (2001) index, with medium-range forecasts that may capture the influence of intraseasonal variations at shorter lead-times.

He and Zhu (2015) investigated the correlations between the SCSSM onset (as determined by the Wang et al. (2004) criteria) and the subsequent EASM rainfall from May

296 to September in observations/reanalyses. They suggested that, in contrast with the
297 traditional view that a later onset date would be associated with a lower than normal total
298 seasonal rainfall amount, the region from the lower Yangtze River to Korea and southern
299 Japan shows a positive correlation between the SCSSM onset date and the seasonal mean
300 rainfall, i.e. early SCSSM onset tends to be followed by lower than normal seasonal mean
301 rainfall further north. He and Zhu (2015) associate this relationship with a persistent
302 Western North Pacific anticyclonic/cyclonic anomaly accompanied by decaying El
303 Niño/La Niña conditions in boreal spring to summer (Wu et al., 2010; Stuecker et al., 2013;
304 Hardiman et al, 2017). This suggests that skilful predictions of SCSSM onset could provide
305 an indication of the seasonal mean rainfall in parts of the EASM region.

306 To our knowledge, this is the first time that skill in predicting the broadscale transition
307 associated with the SCSSM onset on seasonal timescales in an operational dynamical
308 forecasting system has been demonstrated. We encourage other centres to investigate this
309 in their operational forecasting systems. While it is recognised that the onset and
310 progression of the SCSSM and EASM systems is complex and may be influenced by other
311 factors such as synoptic events, intraseasonal variability and regional air-sea interactions
312 with little or no predictability on the seasonal timescale, the ability to provide skilful
313 predictions of whether the broadscale seasonal transition is likely to be early, late or normal
314 provides useful, early information for local forecasters, particularly when combined with
315 other predictions, such as the Yangtze River basin rainfall, which have also been shown to
316 be skilful (Li et al., 2016) and are now provided in real time to CMA (Bett et al., 2018).
317

Acknowledgements: This work and its contributors (GM, AC, RC, ND and AS) were supported by the UK-China Research & Innovation Partnership Fund through the Met Office Climate Science for Service Partnership (CSSP) China as part of the Newton Fund. DZ was supported by the National Natural Science Foundation of China (Grant No. 41605078).

REFERENCES

Adler, R. F., G. J. Huffman, A. Chang, R. Ferraro, P.-P. Xie, J. Janowiak, B. Rudolf, U. Schneider, S. Curtis, D. Bolvin, A. Gruber, J. Susskind, P. Arkin, and E. Nelkin, 2003: The version-2 Global Precipitation Climatology Project (GPCP) monthly precipitation analysis (1979–present). J. Hydrometeor., 4, 1147–1167, https://doi.org/10.1175/1525-7541(2003)004<1147:TVGPCP>2.0.CO;2.

Bett, P., A. A. Scaife, C. Li, C. Hewitt, N. Golding, P. Zhang, N. Dunstone, D. M. Smith, H. E. Thornton, R. Lu, and H. –L. Ren, 2018: Seasonal Forecasts of the Summer 2016 Yangtze River Basin Rainfall. *Adv. Atm. Sci.,* **35**, 918, doi.org/10.1007/s00376-018-7210-y.

Bolton, D., 1980: The computation of equivalent potential temperature. Mon. Wea. Rev., 108, 1046–1053, https://doi.org/10.1175/1520-0493(1980)108<1046:TCOEPT>2.0.CO;2.

Chan, J. C. L., Y. G. Wang, and J. J. Xu, 2000: Dynamic and thermodynamic characteristics associated with the onset of the 1998 South China Sea summer monsoon. J. Meteor. Soc. Japan, 78, 367–380

Dee, D. P., Uppala, S. M., Simmons, A. J., Berrisford, P., Poli, P., Kobayashi, S., Andrae, U., Balmaseda, M. A., Balsamo, G., Bauer, P., Bechtold, P., Beljaars, A. C. M., van

342 de Berg, L., Bidlot, J., Bormann, N., Delsol, C., Dragani, R., Fuentes, M., Geer, A. J.,
343 Haimberger, L., Healy, S. B., Hersbach, H., Hólm, E. V., Isaksen, L., Kållberg, P.,
344 Köhler, M., Matricardi, M., McNally, A. P., Monge-Sanz, B. M., Morcrette, J.-J., Park,
345 B.-K., Peubey, C., de Rosnay, P., Tavolato, C., Thépaut, J.-N. and Vitart, F. 2011: The
346 ERA-Interim reanalysis: configuration and performance of the data assimilation
347 system. *Q.J.R. Meteorol. Soc.*, **137**, 553–597. doi:10.1002/qj.828
348 Ding, Y., and J. C. L. Chan, 2005: The East Asian summer monsoon: an overview. *Meteor.*
349 *Atmos. Phys*., **89**, 117–142, https://doi.org/10.1007/s00703-005-0125-z
350 Ding, Y., and C. He, 2006: The Summer Monsoon Onset over the Tropical Eastern Indian
351 Ocean: The Earliest Onset Process of the Asian Summer Monsoon. *Adv. Atmos. Sci*,
352 **23**, 940–950, doi: 10.1007/s00376-006-0940-2.
353 Dunstone, N., D. Smith, A. Scaife, L. Hermanson, R. Eade, N. Robinson, M. Andrews, and
354 J. Knight, 2016: Skilful predictions of the winter North Atlantic Oscillation one year
355 ahead. *Nature Geosci.* **9**, 809–814, doi:10.1038/ngeo2824.
356 Eade R., D. Smith, A.A. Scaife and E. Wallace, 2014: Do seasonal to decadal climate
357 predictions underestimate the predictability of the real world? *Geophys. Res. Lett.,* **41,**
358 5620-5628, DOI: 10.1002/2014GL061146.
359 Fang, Y., P. Wu, M. S. Mizielinski, M. J. Roberts, T. Wu, B. Li, P. L. Vidale, M. –E.
360 Demory, and R. Schiemann, 2016: High-resolution simulation of the boreal summer
361 intraseasonal oscillation in Met Office Unified model. *Q. J. R. Meteorol. Soc.*, doi:
362 10.1002/qj.2927.
363 Fong, S. K., and A. Y. Wang (Eds.), 2001: *Climatological Atlas for Asian Summer*
364 *Monsoon*. Meteorological and Geophysical Bureau and Macau Foundation, 318 pp.

365 Gao, H., J. He, Y. Tan, and J. Liu, 2001: Definition of 40-year onset date of South China
366 Sea Summer Monsoon. *J. Nanjing Inst. Meteor*., **24**, 379–383.
367 Hardiman, S. C., N. J. Dunstone, A. A. Scaife, P. E. Bett, C. Li, B. Lu, H.-L. Ren, D. M.
368 Smith, and C. C. Stephan, 2018: The asymmetric response of Yangtze river basin
369 summer rainfall to El Niño/La Niña. *Environ. Res. Lett*., **13(2)**, 024015,
370 doi:https://doi.org/10.1088/1748-9326/aaa172
371 He, B., Y. Zhang, T. Li and W.-T. Hu, 2017: Interannual variability in the onset of the
372 South China Sea summer monsoon from 1997 to 2014. *Atmos. and Oc. Sci, Lett.*, **10:1**,
373 73-81, DOI: 10.1080/16742834.2017.1237853
374 He, J. and Z. Zhu, 2015: The relation of South China Sea monsoon onset with the
375 subsequent rainfall over the subtropical East Asia. *Int. J. Climatol.*, **35**: 4547–4556.
376 doi: 10.1002/joc.4305
377 He, Z., and R. Wu, 2013: Seasonality of Interannual Atmosphere–Ocean Interaction in the
378 South China Sea. *J. Oceanography*, **69**, 699–712. doi:10.1007/s10872-013-0201-9
379 Hu, W. T., R. G. Wu, and Y. Liu, 2014: Relation of the South China Sea Precipitation
380 Variability to Tropical Indo-Pacific SST Anomalies during Spring-to-summer
381 Transition. *J. Climate*, **27**, 5451–5467. doi:10.1175/JCLI-D-14-00089.1
382 Kalnay, E., M. Kanamitsu, R. Kister W. Collins, D. Deaven, L. Gandin, M. Iredell, S. Saha,
383 G. White, J. Woollen, Y. Zhu, M. Chelliah, W. Ebisuzakl, W. Higgins, J. Janowiak,
384 K. C. Mo, C. Ropelewski, J. Wang, A. Leetmaa, R. Reynolds, R. Jenne, and D. Joseph,
385 1996: The NCEP/NCAR 40-year reanalysis project. *Bull. Am. Meteorol. Soc.*, **77,** 437–
386 471.

Kanamitsu, M., W. Ebisuzaki, J. Woollen, S. –K. Yang, J. J. Hnilo, M. Fiorino, and G. L. Potter, 2002: NCEP‐DOE AMIP‐II reanalysis (R-2). *Bull. Am. Meteorol. Soc.*, **83**, 1631-1643.

Kumar, A., M. Chen, and W. Wang, 2013: Understanding prediction skill of seasonal mean precipitation over the Tropics. *J. Clim.* **26**, 5674–5681.

Lau, K. M., and S. Yang, 1997: Climatology and interannual variability of the Southeast Asian summer monsoon. *Adv. Atmos. Sci.*, **14**, 141–162

Lee, S. –S., B. Wang, D. E. Waliser, J. M. Neena, and J.-Y. Lee, 2015: Predictability and prediction skill of the boreal summer intraseasonal oscillation in the Intraseasonal Variability Hindcast Experiment. *Climate Dyn.*, **45**, 2123–2135, doi:10.1007/s00382-014-2461-5.

Li, C., A. A. Scaife, R. Lu, A. Arribas, A. Brookshaw, R. E. Comer, J. Li, C. MacLachlan, and P. Wu, 2016: Skilful seasonal prediction of Yangtze river valley summer rainfall. *Environ. Res. Lett.*, **11(9),** 094002, doi:10.1088/1748-9326/11/9/094002.

Li, H., He, S., Fan, K. and Wang, H., 2018: Relationship between the onset date of the Meiyu and the South Asian anticyclone in April and the related mechanisms. *Clim. Dyn.* https://doi.org/10.1007/s00382-018-4131-5

Li, K. P., W. Yu, T. Li, V. S. N. Murty, S. Khokiattiwong, T. R. Adi, and S. Budi, 2013: Structures and mechanisms of the first-branch northward-propagating intraseasonal oscillation over the tropical Indian Ocean. *Clim. Dyn.*, **40**, 1707–1720

Li, R. C. Y., W. Zhou, and T. Li, 2014: Influences of the Pacific–Japan Teleconnection Pattern on Synoptic-Scale Variability in the Western North Pacific. *J. Clim.*, **27**, 140–154, doi:10.1175/JCLI-D-13-00183.1

410 Lim, Y., S. Son, and D. Kim, 2018: MJO prediction skill of the Subseasonal-to-Seasonal
411 Prediction models. *J. Clim.*, **31**, 4075–4094, https://doi.org/10.1175/JCLI-D-17-
412 0545.1
413 Liu, Y., J. C. L. Chan, J. Mao, and G. Wu, 2002: The role of Bay of Bengal convection in
414 the onset of the 1998 South China Sea summer monsoon. Mon. Wea. Rev., 130, 2731–
415 2744, doi:https://doi.org/10.1175/1520-0493(2002)130<2731:TROBOB>2.0.CO;2
416 Luo, M. and L. Lin, 2017: Objective determination of the onset and withdrawal of the
417 South China Sea summer monsoon. *Atmos. Sci. Lett.*, **18**, 276–282.
418 doi:10.1002/asl.753
419 Luo, M., Y. Leung, H.F. Graf, M. Herzog, and W. Zhang, 2016: Interannual variability of
420 the onset of the South China Sea summer monsoon. *Int. Jou. Clim.,* **36**, 550–562
421 Luo, Y., H. Wang, R. Zhang, W. Qian, and Z. Luo, 2013: Comparison of rainfall
422 characteristics and convective properties of monsoon precipitation systems over south
423 China and the Yangtze and Huai River basin. *J. Climate*, **26**, 110–132,
424 doi:https://doi.org/10.1175/JCLI-D-12-00100.1.
425 MacLachlan, C., A. Arribas, A. K. Peterson, A. Maidens, D. Fereday, A. A. Scaife, M.
426 Gordon, M. Vellinga, A. Williams, R. E. Comer, J. P. Camp, Xavier, and G. Madec,
427 2015: Global Seasonal forecast system version 5 (GloSea5): a high-resolution seasonal
428 forecast system. *Q.J.R. Meteorol. Soc.*, **141**, 1072–1084. doi:10.1002/qj.2396
429 Rayner, N. A., D. E. Parker, E. B. Horton, C. K. Folland, L. V. Alexander, D. P. Rowell,
430 E. C. Kent, and A. Kaplan, 2003: Global analyses of sea surface temperature, sea ice,
431 and night marine air temperature since the late nineteenth century. *J. Geophys. Res.*,
432 **108**, 4407

433 Saha K., 2010: Monsoon over Eastern Asia (Including China, Japan, and Korea) and
434 Adjoining Western Pacific Ocean. *Tropical Circulation Systems and Monsoons*. K.
435 Saha, Ed., Springer, Berlin, Heidelberg, 123-153.
436 Sampe, T., and Xie S. P. 2010: Large-scale dynamics of the Meiyu–Baiu rainband:
437 environmental forcing by the westerly jet. *J. Clim*., **23**, 113–134
438 Scaife, A. A., A. Arribas, E. Blockley, A. Brookshaw, R. T. Clark, N. Dunstone, R. Eade,
439 D. Fereday, C. K. Folland, M. Gordon, L. Hermanson, J. R. Knight, D. J. Lea, C.
440 MacLachlan, A. Maidens, M. Martin, A. K. Peterson, D. Smith, M. Vellinga, E.
441 Wallace, J. Waters, A. Williams, 2014: Skilful long-range prediction of European and
442 North American winters, *Geophys. Res. Lett.*, **41**, 2514–2519,
443 doi:10.1002/2014GL059637.
444 Scaife, A.A., R. E. Comer, N. J. Dunstone, J. R. Knight, D. M. Smith, C. MacLachlan, N.
445 Martin, A. K. Peterson, D. Rowlands, E. B. Carroll, S. Belcher, and J. Slingo, 2017:
446 Tropical Rainfall, Rossby Waves and Regional Winter Climate Predictions. *Quart. J.*
447 *Roy. Met. Soc.*, **143**, 1-11. doi:10.1002/qj.2910.
448 Shao, X., P. Huang, and R. -H. Huang, 2014: Role of the phase transition of intraseasonal
449 oscillation on the South China Sea summer monsoon onset. *Clim. Dyn.,* **45**, 125–137.
450 Stuecker, M. F., A. Timmermann, F. –F. Jin, S. McGregor, and H. –L. Ren, 2013: A
451 Combination mode of the annual cycle and the El Niño/Southern Oscillation. *Nat*
452 *Geosci,* **6,** 540–544.
453 Tao, S-Y., and L-X. Chen, 1987: Review of recent research on the East Asian summer
454 monsoon in China. *Monsoon Meteorology*, C.-P. Chang and T. N. Krishnamurti, Eds.,
455 Oxford University Press, 60–92.

456 Wang, B., F. Huang, Z. Wu, j. Yang, X. Fu, and K. Kikuchi, 2009: Multi-scale climate
457 variability of the South China Sea monsoon: a review. *Dyn. Atmos. Oceans*., **47,** 15–
458 37
459 Wang, B., Y. Zhang, and M. M. Lu, 2004: Definition of South China Sea monsoon onset
460 and commencement of the East Asia summer monsoon. *J. Clim.*, **17**, 699–710.
461 Wang, H., F. Liu, B. Wang, and T. Li, 2017: Effects of intraseasonal oscillation on South
462 China Sea summer monsoon onset. *Clim. Dyn.*, doi:10.1007/s00382-017-4027-9.
463 Weisheimer, A., and T. N. Palmer, 2014: On the reliability of seasonal climate forecasts.
464 *J. R. Soc. Interface,* **11**, 20131162, doi: 10.1098/rsif.2013.1162.
465 Williams, K. D., C. M. Harris, A. Bodas-Salcedo, J. Camp, R. E. Comer, D. Copsey, D.
466 Fereday, T. Graham, R. Hill, T. Hinton, P. Hyder, S. Ineson, G. Masato, S. F. Milton,
467 M. J. Roberts, D. P. Rowell, C. Sanchez, A. Shelly, B. Sinha, D. N. Walters, A. West,
468 T. Woollings, and P. K. Xavier, 2015: The Met Office Global Coupled model 2.0 (GC2)
469 configuration, *Geosci. Model Dev.*, **8**, 1509-1524, https://doi.org/10.5194/gmd-8-
470 1509-2015.
471 Wu, R., 2010: Subseasonal variability during the South China Sea monsoon onset. *Clim.*
472 *Dyn.*, **34**, 629–642, doi:10.1007/s00382-009-0679-4.
473 Xie, S. P., Y. Kosaka, Y. Du, and G. Huang, 2015: Indo-western Pacific ocean capacitor
474 and coherent climate anomalies in post-ENSO summer: a review. *Adv. Atmos. Sci.*,
475 doi:10.1007/s00376-015-5192-6
476 Zhou, W., and J. C. L. Chan, 2007: ENSO and the South China Sea Summer Monsoon
477 Onset. *Int. Jou. Climatol.,* **27**, 157–167.10.1002/(ISSN)1097-0088

Zhu, Z., and J. He, 2013: The vortex over Bay of Bengal and its relationship with the outbreak of South China Sea summer monsoon. *J. Trop. Meteor*., **71 (3)**, 915-923

Zhu, Z., and T. Li, 2017: Empirical prediction of the onset dates of South China Sea summer monsoon. *Clim. Dyn*., **48 (5)**, 1633-1645, doi:10.1007%2Fs00382-016-3164-x

FIGURE CAPTIONS

Figure 1: Predictability of the SCSSM wind onset: onset pentads derived using the method proposed by Wang et al. (2004) from the GloSea5 ensemble predictions initialized on 17th, 25th March, 1st, 9th April (green dots represent individual members of the 52-member ensemble, with the size of the dot scaled by the number of members predicting the same onset pentad) and their ensemble mean (green line) compared with the equivalent onset pentads derived from ERA-Interim (black line). The yellow line shows the Niño3.4 SST anomaly in March for each year taken from the HadISST1.1 dataset. Pearson correlation coefficients are given in the legend: r(ens,obs) represents the correlation between the GloSea5 ensemble mean and ERA-Interim; r(ens,sst) represents the correlation between the GloSea5 ensemble mean SCS onset pentads and the observed March Niño3.4 SST anomaly; r(obs,sst) represents the correlation between the ERA-Interim SCS onset pentads and the observed March Niño3.4 SST anomaly.

Figure 2: As Fig. 1 but for SCSSM thermodynamic onset as determined by a sustained increased of $\theta_{e,SCS}$ above 340K accompanied by the establishment of westerly winds

over the region 10-20N 110-120E, as proposed by Gao et al. (2001) (with the threshold modified by Ding and He, 2006).

Figure 3: Correlation coefficients between SCSSM onset pentad derived using the Wang et al. (2004) index and observed March average sea surface temperatures from HadISST1.1 for the period 1993-2015, using: (a) ensemble mean onset dates from the hindcast; (b) onset dates from ERA-Interim, (c) 10,000 pseudo-timeseries of onset dates created by randomly selecting an individual ensemble member from each year; panel shows average over all correlations. Contours and darker shades indicate correlations significant at the 1% (r=0.48) and 3% (r=0.40) levels respectively, for a one-tailed t-test.

Figure 4: Effect of ensemble size on the skill of SCSSM onset predictions using the Wang et al. (2004) index (solid line), denoted r(ens,obs), and the signal to noise ratio (correlation of ensemble mean timeseries with a pseudo-timeseries created by randomly selecting a single model ensemble member for each year, dashed line), denoted r(ens,mod). In both cases, for each choice of ensemble size, up to 10,000 ensemble-mean timeseries are generated by randomly selecting the chosen number of ensemble member onset dates (independently and without replacement) from the 52 onset dates diagnosed in each year in the combined ensemble and averaging over the chosen number of ensemble members. Dot-dashed lines indicate the values of r that are significant at the 1% and 0.1% levels for a one-tailed t-test.

521 **Table 1.** Pearson correlation coefficients between ensemble mean SCSSM onset dates
522 from GloSea5 and those from ERA-Interim, using the definitions of Wang et al. (2004)
523 and Gao et al. (2001), for different hindcast start dates. Note that the earliest observed
524 SCSSM onset date is pentad 25 (1^{st} -5^{th} May) and the mean onset date is pentad 28 (16^{th}-
525 20^{th} May). Where just the month is shown, start dates are 1^{st}, 9^{th}, 17^{th}, and 25^{th} of the month.
526 Correlation coefficients statistically significant (for a 23 year hindcast period) at <1.5%
527 level for a 1-tailed test are in *italics* and those significant at <1% level for a 1-tailed test
528 are in **bold.**

	Ensemble start dates				
	January	February	March	17^{th}, 25^{th} March, 1^{st}, 9^{th} April	25^{th} March, 1^{st}, 9^{th}, 17^{th} April
Wang et al. (2004)	0.28	*0.46*	*0.45*	**0.50**	**0.53**
Gao et al. (2001)	-	-	-	0.27	0.30

529

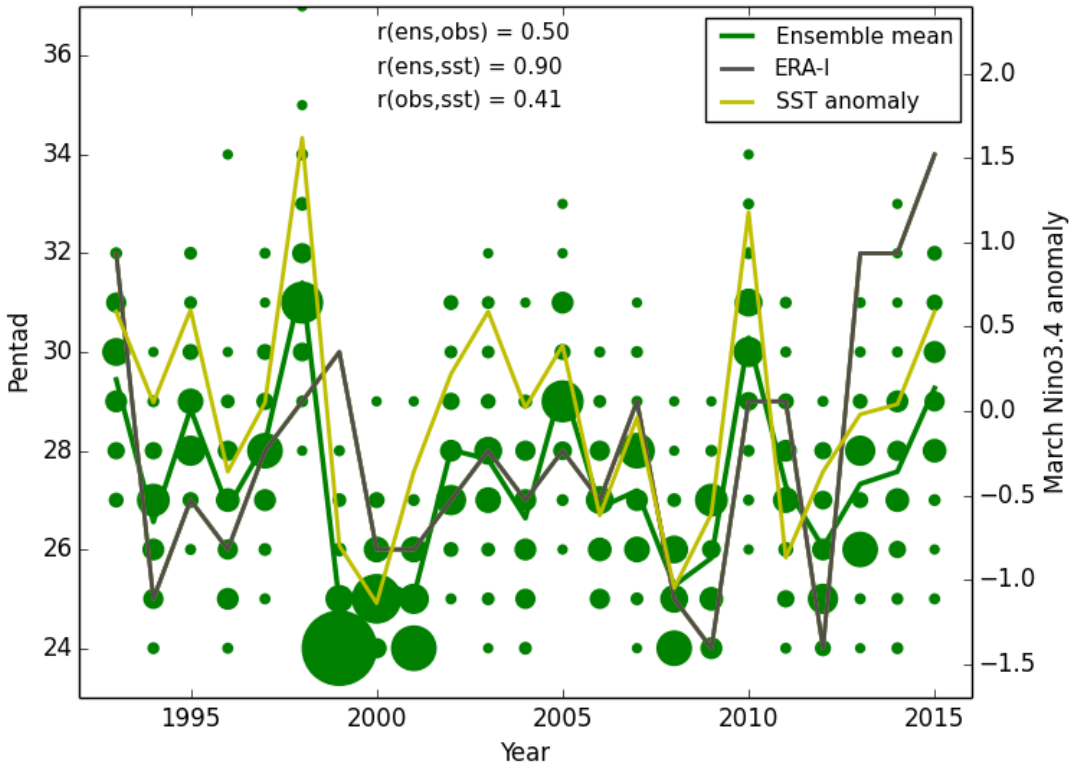

Fig. 1: Predictability of the SCSSM wind onset: onset pentads derived using the method proposed by Wang et al. (2004) from the GloSea5 ensemble predictions initialized on 17th, 25th March, 1st, 9th April (green dots represent individual members of the 52-member ensemble, with the size of the dot scaled by the number of members predicting the same onset pentad) and their ensemble mean (green line) compared with the equivalent onset pentads derived from ERA-Interim (black line). The yellow line shows the Niño3.4 SST anomaly in March for each year taken from the HadISST1.1 dataset. Pearson correlation coefficients are given in the legend: r(ens,obs) represents the correlation between the GloSea5 ensemble mean and ERA-Interim; r(ens,sst) represents the correlation between the GloSea5 ensemble mean SCS onset pentads and the observed March Niño3.4 SST

anomaly; r(obs,sst) represents the correlation between the ERA-Interim SCS onset pentads and the observed March Niño3.4 SST anomaly.

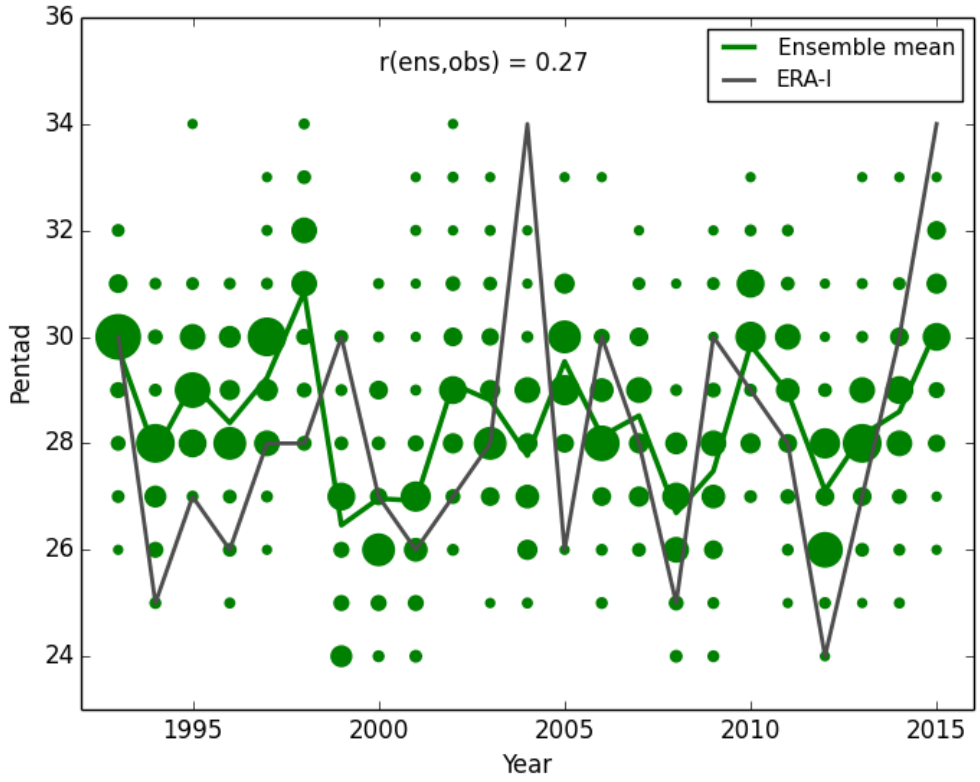

Fig. 2: As Fig. 1 but for SCSSM thermodynamic onset as determined by a sustained increased of $\theta_{e,SCS}$ above 340K accompanied by the establishment of westerly winds over the region 10-20N 110-120E, as proposed by Gao et al. (2001) (with the threshold modified by Ding and He, 2006).

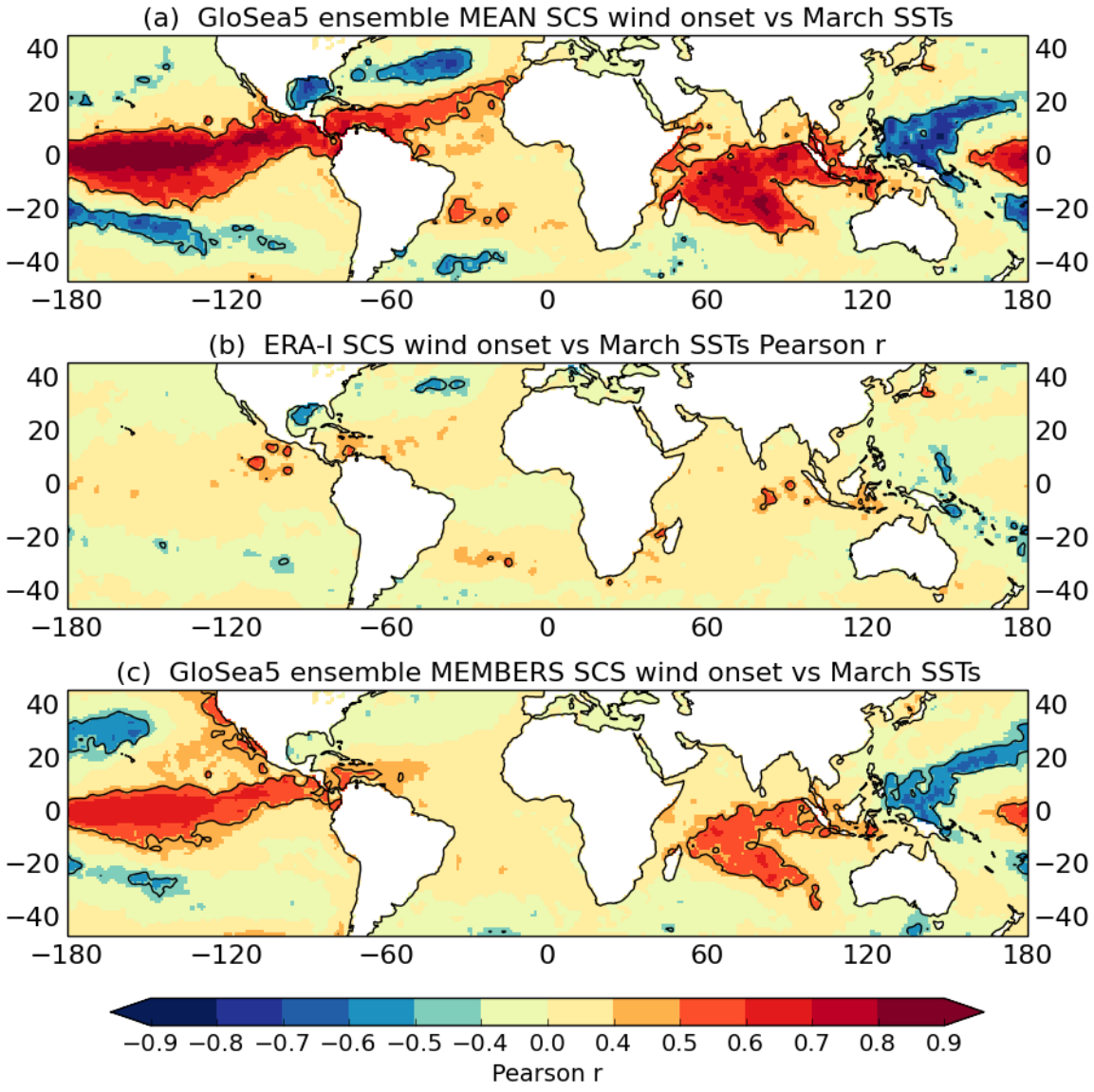

551

552 **Fig. 3:** Correlation coefficients between SCSSM onset pentad derived using the Wang et
553 al. (2004) index and observed March average sea surface temperatures from HadISST1.1
554 for the period 1993-2015, using: (a) ensemble mean onset dates from the hindcast; (b) onset
555 dates from ERA-Interim, (c) 10,000 pseudo-timeseries of onset dates created by randomly
556 selecting an individual ensemble member from each year; panel shows average over all
557 correlations. Contours and darker shades indicate correlations significant at the 1%
558 (r=0.48) and 3% (r=0.40) levels respectively, for a one-tailed t-test.

559

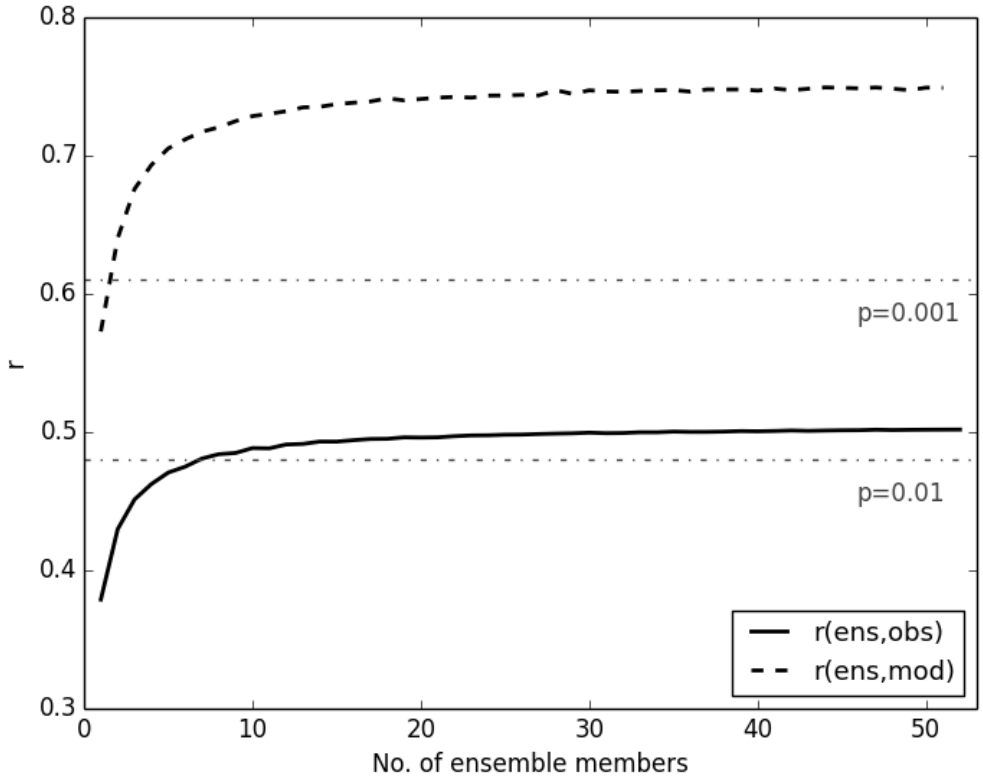

560

561 **Fig. 4**: Effect of ensemble size on the skill of SCSSM onset predictions using the Wang
562 et al. (2004) index (solid line), denoted r(ens,obs), and the signal to noise ratio
563 (correlation of ensemble mean timeseries with a pseudo-timeseries created by randomly
564 selecting a single model ensemble member for each year, dashed line), denoted
565 r(ens,mod). In both cases, for each choice of ensemble size, up to 10,000 ensemble-mean
566 timeseries are generated by randomly selecting the chosen number of ensemble member
567 onset dates (independently and without replacement) from the 52 onset dates diagnosed
568 in each year in the combined ensemble and averaging over the chosen number of
569 ensemble members. Dot-dashed lines indicate the values of r that are significant at the
570 1% and 0.1% levels for a one-tailed t-test.